Characterization and Application of Nanomaterials 2024, 7(1), 5593.
https://doi.org/10.24294/can.v7i1.5593

Article

Green recovery of NaF-Na_2CO_3-NaCl ternary fluxing agent from aluminum dross

Mostafa Mahinroosta[1,2,*], Ali Allahverdi[2]

[1] Department of Energy, Materials and Energy Research Center, Karaj 3177983634, Iran
[2] Research laboratory of Inorganic Chemical Process Technologies, School of Chemical Engineering, Iran University of Science and Technology, Tehran 1684613114, Iran
*** Corresponding author:** Mostafa Mahinroosta, mahinroosta2010@gmail.com

CITATION

Mahinroosta M, Allahverdi A. Green recovery of NaF-Na_2CO_3-NaCl ternary fluxing agent from aluminum dross. Characterization and Application of Nanomaterials. 2024; 7(1): 5593. https://doi.org/10.24294/can.v7i1.5593

ARTICLE INFO

Received: 18 December 2023
Accepted: 6 March 2024
Available online: 1 April 2024

Abstract: The present study deliberates the recovery of sodium fluoride (NaF)-natrite (Na_2CO_3)-sodium chloride (NaCl) ternary fluxing agent from hazardous aluminum dross waste using three types of heating methods, including direct heating on a hotplate, heating by a drying oven, and microwave heating. Deionized water was used as a green solvent for the recovery experiments. Investigating the effects of time and temperature on recovery percentage showed that a recovery percentage of around 96.5% can be achieved under time and temperature of 90 min and 95 °C, respectively. The recovered fluxing agent salt was characterized by XRD, FTIR spectroscopy, FESEM, and energy dispersive X-ray spectroscopy (EDS) elemental analysis. Rietveld fitting analysis of phases detected in the XRD patterns showed that the recovered fluxing agent contained 74–81 wt.% NaF, 8–11 wt.% NaCl, and 11–14.7 wt.% Na_2CO_3. The FESEM micrographs revealed that the retrieved salts were in nano scale. The recovered fluxing agent showed different morphologies including needle-like, round shape, and a mixture of both, corresponding to microwave, drying oven, and hotplate heating methods, respectively. The nano-needles exhibited diameter of the tip and base in the range of 39–60 nm and 50–103 nm, respectively.

Keywords: waste; sodium fluoride; needle-like; microwave-assisted; nanostructure

1. Introduction

With a general look at the current situation of the industry in the world, industrial production is associated with challenging issues such as waste accumulation and natural resource depletion. The accumulation of industrial wastes over time generates environmental and public health problems [1]. In recent years, public awareness on improving the quality and preservation of the environment has coerced legislators into passing strict regulations on air and water pollution [2].

Aluminum black dross (ABD) as a hazardous industrial waste is a salty-metallic-oxidic waste of aluminum ingot production process formed in casting units [3,4]. The ABD also contains about 8%–10% of soluble salts, mainly alkali fluorides and chlorides [5,6]. In aluminum production process, a fluxing agent (usually a salt mixture containing sodium and potassium chlorides as well as a small amount of a mineral fluorine compounds (Na_3AlF_6 or CaF_2) is used to protect Al metal from oxidation under favorable conditions (high temperature and the presence of oxygen) [1]. NaF is formed as a result of the disintegration of Na_3AlF_6 (also known as cryolite) which plays the role of an electrolyte in the melting process as well as a fluxing agent in the process of smelting alumina and turning it into metallic aluminum [7,8]. Also, NaF may directly come from the molten salt flux [7].

In Europe, stockpiling of this kind of waste is prohibited because the soluble salts are a major source of surface and groundwater pollution [9] and may have some disadvantages such as cost and safety risks [5,6]. The presence of excess fluoride in drinking water often results in skeletal fluorosis, weakening bone structure, as well as discoloration and speckling of teeth, cancer or adverse effects on the brain and kidney [10]. Also, high levels of sodium in drinking water exacerbate chronic congestive heart failure, blood pressure and hypertension [11]. Therefore, finding an appropriate solution to eliminate or reduce the environmental pollution of the waste is a necessity.

Halite (NaCl), natrite (Na_2CO_3), and NaF are water-soluble and recoverable mineral salts. The recovered salt can be mixed with fresh fluxing agent and returned to aluminum smelting furnace. This is economically beneficial and also reduces the toxicity of the ABD waste [12]. Recently, NaF pellets have been applied for the adsorption of gaseous HF as an impurity in the industrial generation of fluorine gas [13]. Inasmuch as the adsorption of gaseous pollutants can be noticeably enhanced by developing nano-structures [14], the last mentioned application of NaF seems more important.

NaF in a bulk scale is prepared by neutralizing hydrofluoric acid with sodium hydroxide [15]. In nano scale, the synthesis of nanoparticles of sodium halide salts (NaF; NaCl, NaBr, NaI) having sizes of less than 3.0 nm using reverse micelles methods with capping agent has been reported by Abdelkader and Buckner [16].

Sodium carbonate (Na_2CO_3) can be used to remove iron oxide in some stages of aluminum production and cause further purification of aluminum. In addition, sodium carbonate can improve the flotation performance and play a role as a pH regulator [17]. In the aluminum smelting process, sodium carbonate improves the performance of the fluxing agent [18]. Sodium fluoride, sodium chloride, and sodium carbonate can be used as roasting agents in the processes of extracting valuable materials from primary and secondary sources [19–21].

Within the scope of this work, facile green recovery of fluxing agent nanostructures from the ABD is investigated for the first time. The recovery of soluble salts in the form of nanostructures implies to the principles 3 (substances with little or no hazard), 5 (safer solvents and auxiliaries), and 12 (safety considerations) of the twelve principles of green chemistry [22]. After removing the soluble salts from the ABD, its pollution is significantly reduced, and the soluble salt-free residue can be subjected to subsequent processes such as the recovery of alumina as a valuable and widely used material [23,24].

2. Materials and methods

2.1. Materials

The ABD used herein was obtained from Iranian Aluminum Company (Iralco) situated in Markazi province, Iran. The as-received BAD was medium gray in color with the actual and bulk densities of 2.22 and 0.85 g/cm^3, respectively. The mineralogy of the ABD will be discussed in section 3.2. **Figure 1** shows the particle size distribution of the ABD. As seen, about 55% of the ABD particles are below 250 μm, whereas about 90% of which are less than 2.38 mm.

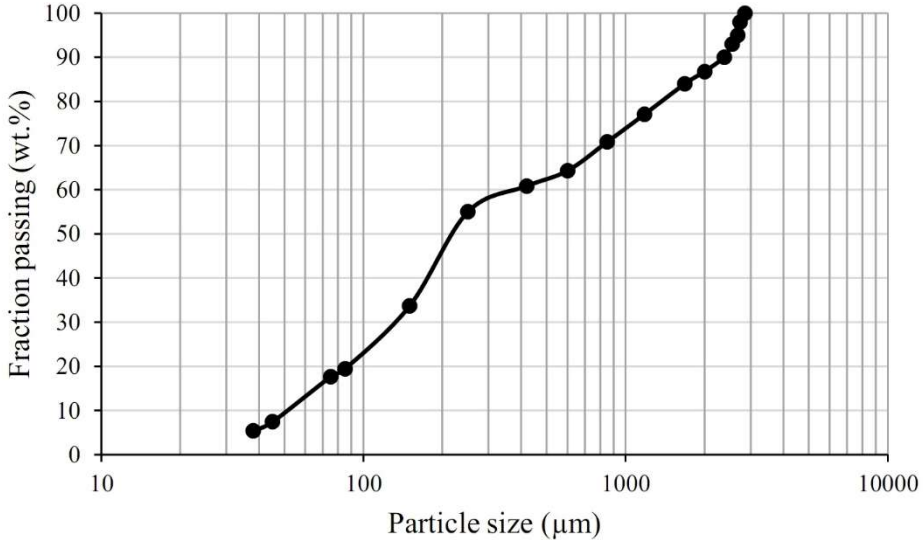

Figure 1. Particle size distribution of ABD.

Table 1 gives oxide composition of the ABD which was determined by X-ray fluorescence (XRF) technique. According to data in **Table 1**, the ABD contains almost 61 and 15 wt.% aluminum oxide and silicon dioxide, respectively. The loss on ignition (LOI) was obtained around 9 wt.% and the remaining 15 wt.% accounts for the other oxides.

Deionized (DI) water (TDS = 5 mg/L) was utilized at all recovery experimental tests as a green solvent.

Table 1. Chemical composition of ABD.

Oxide	**(wt.%)**
Al_2O_3	62.56
SiO_2	7.53
CaO	5.87
Fe_2O_3	2.73
Na_2O	4.68
MgO	1.25
P_2O_5	0.17
SO_3	0.10
K_2O	0.81
TiO_2	0.32
MnO	0.31
Cl	3.35
F	1.32
CuO	0.11
LOI*	8.89

2.2. Methods

2.2.1. Determination of water leachable salt content of ABD

To determine the water leachable salt content of the ABD, the method described in DIN 38414-S4 standard for determination of leachability by water was used. According to this standard, first 100 g of dry ABD sample is loaded into a 2 L beaker and then 1 L of DI water is added. The mixture is then stirred for 24 h. After the mixing time has elapsed, the mixture is filtered through a vacuum filtration system. The filtrate should be transparent at this stage, otherwise it must be re-filtered with a filter paper with a mesh size of 0.45 μm. The determination of the chemical analysis of leachate is performed using inductively coupled plasma atomic emission spectroscopy (ICP-AES). At the end of the experiment, the mass of the leached substance is calculated by the following Equation (1).

$$W_{ES} = (\beta \times V_E)/m_s \quad (1)$$

where, W_{ES} is the mass of the leached substance (in mg/kg), β is the mass concentration of the leached substance (in mg/L), m_s is the dry mass of initial sample (in kg), and V_E is the volume of the filtrate (in L).

2.2.2. Salt recovery experiments

To perform salt recovery experiments, the setup shown in **Figure 2** was used. **Figure 2** shows a three-neck glass reactor, Graham condenser, a water bath for homogenizing the recovery temperature, and a magnetic stirrer. After accurate weighing, 5.00 g of the ABD is loaded into the reactor. Then 100 mL of deionized water is added to it. The rinsing starts at a specified temperature under the stirring speed of 600 rpm. After a certain period of time, the suspension is filtered using a vacuum filtration system.

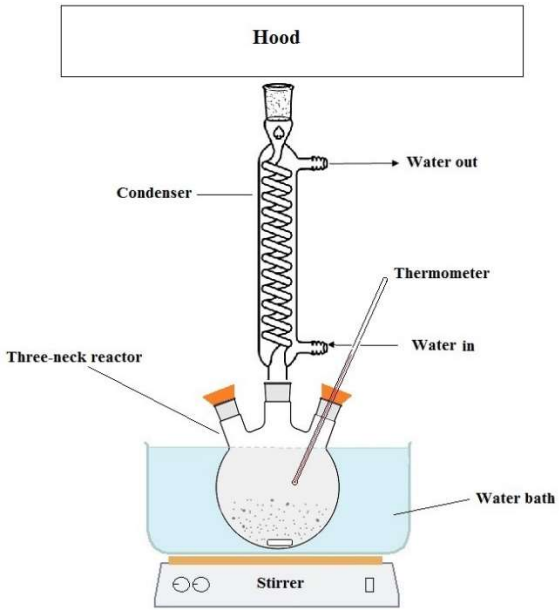

Figure 2. Experimental setup used for salt recovery from ABD.

As illustrated in **Figure 3**, in order to evaporate the water content of the obtained filtrate, three types of heating methods including microwave irradiation, heating by a drying oven (Pars Khazar, OT 650P), and heating by a hotplate (IKA C-MAG HS7

Digital) were applied. The microwave irradiation was provided using a domestic microwave oven (Sapor, 1500 W, 2450 MHz). At the end of the heating, a white solid was achieved. The heating processes were performed at 95 ± 1 ℃ for 2 h by hotplate and at 95 ± 0.5 ℃ for 1 h by drying oven. The microwave irradiation continued for a preset time of 15 min.

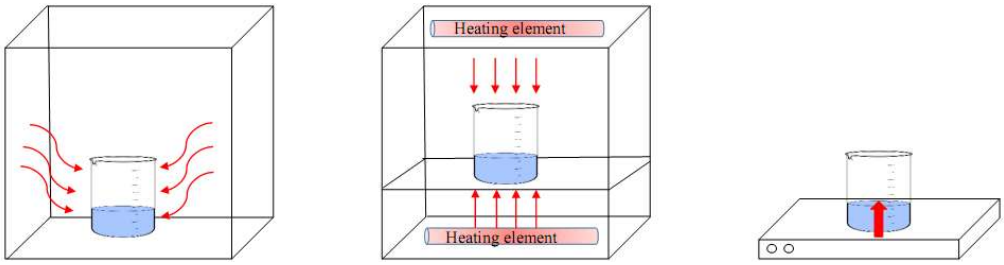

Figure 3. Three types of heating methods (left: microwave irradiation, middle: heating by a drying oven, right: heating by a hotplate).

2.2.3. Characterization methods

To obtain X-ray diffractograms of the samples, Philips Expert System X-ray diffractometer was utilized with CuKα-radiation and Ni-filter at voltage and current of 40 kV and 30 mA, respectively. The XRD analyses were carried out at 2θ angles of 10°–80° (scanning speed: 2 °/min; anti-scatter: 1°; receiving slit: 0.01 mm). Fourier transform infrared spectroscopy (FTIR) spectra of the recovered salts were recorded employing a FTIR spectrometer device (SHIMADZU IR Spectrophotometer 8400 s) in the wavenumber range of 400–4000 cm^{-1}. The spectra were recorded with a sensitivity of 4 cm^{-1} and 64 scans per spectrum taken.

Morphological and elemental analyses were obtained employing two kinds of microscopes including SIGMA VP-500 FESEM microscope (ZEISS) and TESCAN MIRA3 at accelerating voltages of 15 and 10 kV, respectively. For sample preparation, an adequate amount of the recovered salts is adhered on a holder. Then they are coated with a thin layer of gold. The chemical composition of the ABD was determined using a XRF PW2404 device with a measurement range of 20 ppm to 100 wt.%.

3. Results and discussion

3.1. Chemical analysis of leachate

The ICP-AES chemical analysis of the leachate obtained according to DIN 38414-S4 standard is presented in **Table 2**, indicating significant amount of sodium and minor amounts of potassium and aluminum.

Table 2. Chemical analysis of the leachate obtained according to DIN 38414-S4 standard.

Element	Na	K	Al	Ca
Concentration (mg/L)	5662.40	37.23	74.77	ND*
Mass%	98.06	0.64	1.30	-

*ND: not detected.

Based on the data in **Table 2**, the water leachable salt content of the ABD was 5.77 mass%. The pH value of the leachate was around 11.25.

The previous studies [23,24] revealed that the ABD contains aluminum oxide (Al_2O_3), spinel ($MgAl_2O_4$), quartz (SiO_2), diaoyudaoite ($NaAl_{11}O_{17}$), villiaumite (NaF), cryolite (Na_3AlF_6), silicon (Si), aluminum nitride (Al) and iron oxide (Fe_2O_3) as well as minor traces of halite (NaCl), graphite (C), and fluorite (CaF_2). Considering the aforementioned compounds, the presence of sodium in the leachate is majorly due to the dissolution of NaF and NaCl. The presence of aluminum in the leachate originates from the partial hydrolysis of aluminum nitride in water [25,26]. A trace amount of potassium is more likely due to the dissolution of potassium chloride which is used along with sodium chloride as salt flux in melting process of aluminum.

3.2. Effects of time and temperature on salt recovery efficiency

Before performing any salt recovery experiment, the moisture content of the ABD sample was removed in a drying oven at 105 ± 0.5 ℃. This is a necessary step to obtain exact recovery efficiency data. The previous study [24] showed that a drying time of 50 min is enough to completely remove the moisture. In order to investigate the possibility of faster recovery of soluble salts, water leaching of the ABD was carried out at different temperatures and times. In these experiments, the water leaching of the ABD was performed at 25, 45, 65, 85 and 95 ℃ for 30, 60, 90, and 120 min at each temperature. Each experiment was performed twice. The results are depicted in **Figure 4**.

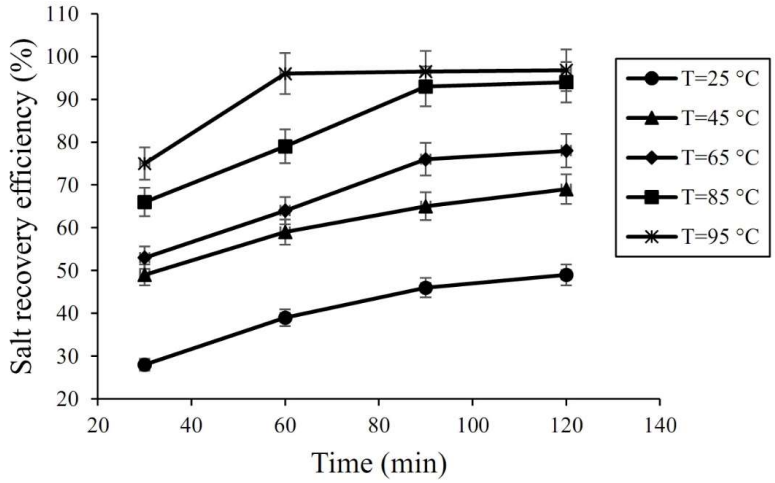

Figure 4. The effects of time and temperature on salt recovery efficiency.

From **Figure 4**, it is clear that the salt recovery efficiency generally increases with increasing temperature and time. Such an enhancement was expected, since the solubility of NaF in water increases with temperature [27]. At 95 ℃, after 60 min, the recovery efficiency is about 96%, and more increase in time does not significantly change the percentage of salt recovery. Also, recovery times of more than 1 h are not practically interesting. **Figure 5** shows the XRD patterns of the raw ABD and water-leached ABD.

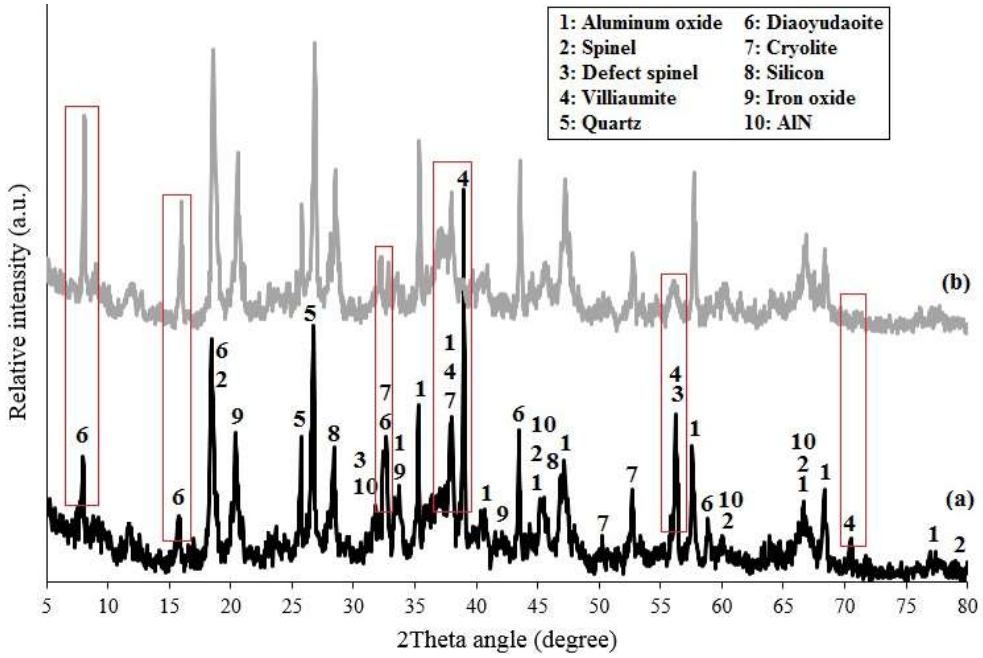

Figure 5. XRD patterns of **(a)** raw ABD and **(b)** water-leached ABD.

Figure 5a shows that the ABD contains aluminum oxide (Al_2O_3), spinel ($MgAl_2O_4$), defect spinel ($Al_{1.83}Mg_{0.87}O_{3.61}$), quartz ($SiO_2$), diaoyudaoite ($NaAl_{11}O_{17}$), villiaumite (NaF), cryolite (Na_3AlF_6), silicon (Si), aluminum nitride (Al) and iron oxide (Fe_2O_3) as well as minor traces of halite (NaCl), graphite (C), and fluorite (CaF_2). Among all these phases, only NaF and NaCl are highly soluble in water. As can be clearly observed from the peaks surrounded by rectangles in **Figure 5**, almost all villiaumite (NaF) has been dissolved in water. Reduced intensity of the diaoyudaoite phase shows that this phase has also partially been dissolved in water. Unfortunately, there is not enough information on the solubility of this material in the literature.

3.3. Characterization of the recovered salts

3.3.1. XRD patterns

Figure 6 presents the X-ray diffractograms of the recovered salts using the mentioned three types of heating methods. The peaks of the recovered salts correspond to those of NaF, NaCl, KCl, AlN, and SiO_2 phases according to the standard cards of ICDD-01-089-2956, ICDD-01-088-2300, ICDD-01-077-2121, ICDD-01-089-3446, and ICDD-01-081-0069, respectively. Because XRD data are substantially qualitative and also due to the proximity of the intensities of some peaks, a reasonable comparison between the three patterns requires the quantification of data and gaining the mass fraction of each phase. To calculate the mass fraction of each phase, the XRD data were quantified applying the Rietveld fitting analysis. The Rietveld fitting analyses were performed using crystallographic information files (CIFs) of villiaumite (NaF), halite (NaCl), and natrite (Na_2CO_3). According to the quantitative data shown in **Figure 6**, the recovered salts consist of predominantly NaF, accounting for 74–81 wt.%. The remaining 20–25 wt.% is dedicated to the presence of sodium chloride and sodium carbonate. The higher amount of NaF improves the performance of fluxing agent. Therefore, according to **Figure 6**, heating by a drying oven is more suitable. In

fact, this type of drying method is a type of indirect heating method, which is mainly done through convection.

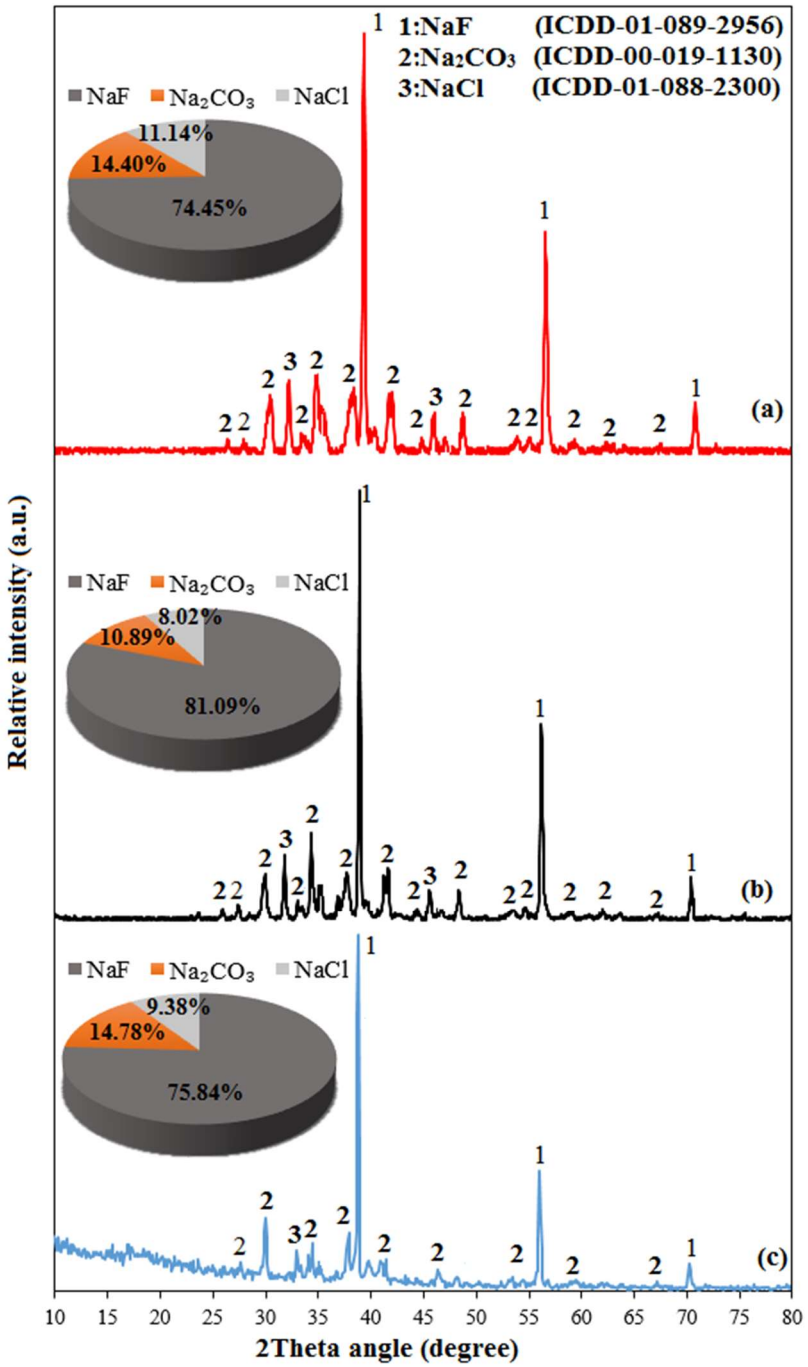

Figure 6. XRD patterns of the recovered salts. Heat source: **(a)** microwave irradiation, **(b)** drying oven, and **(c)** hotplate.

The average crystallite size was obtained using Scherrer equation:

$$L = k\lambda/\beta\cos\theta \quad (2)$$

in which L is the average crystallite size, θ the Bragg's angle, λ the incident X-ray wavelength (λ = 1.541874 Å), and β the full width at half maximum (FWHM) of the peak. β and 2θ values were obtained from each XRD pattern using HighScore Plus software. The results are presented in **Table 3**.

Table 3. Values of 2θ, β, and average crystallite size of the recovered salts.

Recovered salt sample	2θ (degree)	β (degree)	β (rad)	Average crystallite size (nm)
Salt recovered by microwave irradiation	38.9254	0.1653	0.00288	61.9
Salt recovered by drying oven heating	38.9232	0.1968	0.00343	52.0
Salt recovered by hotplate heating	38.7726	0.2952	0.00515	34.5

According to **Table 3**, the salt recovered by hotplate heating has the most minute average crystallite size (34.5 nm) and the salt recovered by microwave irradiation has the largest one (61.9 nm). The larger crystal size of the salt recovered by microwave irradiation is due to the fact that the heating rate is very rapid (only one tenth to one hundredth of the time needed by conventional ways), which leads to the supersaturation of the solution. Crystals in a supersaturated solution can grow faster and become larger [28,29].

3.3.2. FTIR analysis

Figure 7 depicts FTIR spectra of the recovered salts.

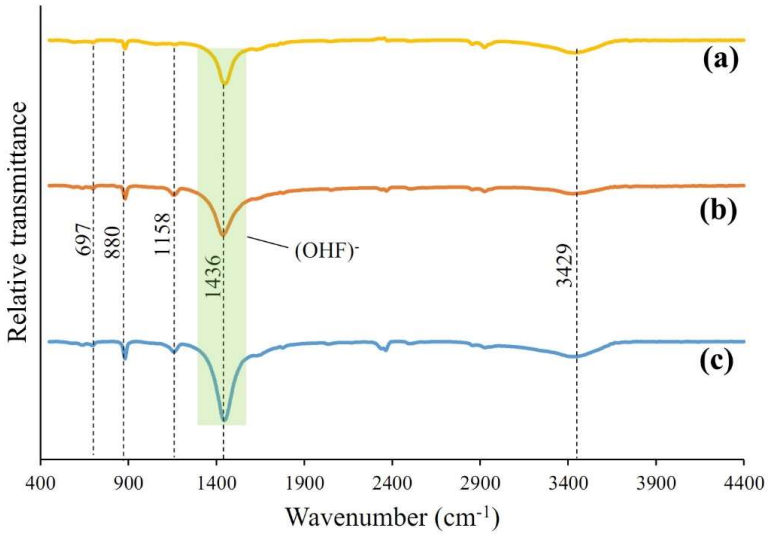

Figure 7. FTIR spectra of the recovered salts. Heat source: **(a)** microwave irradiation; **(b)** drying oven; and **(c)** hotplate.

All three samples show absorption bands at 697, 880, 1158, 1436, 2366, 2924, and 3429 cm^{-1}. The bands observed at 697 and 880 cm^{-1} are assigned to the presence of AlN. This is in agreement with the literature that the main excitation of the Al-N bonds by infrared radiation take place at the range 200-1000 cm^{-1} [30]. The band at 1158 cm^{-1} is caused by the asymmetric stretching of the oxygen atom in the Si-O-Si chain [31]. The absorption band at 1436 cm^{-1} is allocated to $(OHF)^-$ complexes with a hydrogen bond [32,33]. The presence of $(OHF)^-$ complex may be due to some amount of water at the surface of the recovered salts, which dissolves some NaF and produces fluoride ions. Thus, the generated fluoride ions are surrounded by OH groups due to hydrogen bonding. Considering this peak, it is realized that its intensity in the salt recovered by hotplate heating is higher than that in two other samples. The reason

may be the formation of more hydrogen bonds and thus the formation of more $(OHF)^-$ complexes. This evidence suggests that the hotplate heating method is less effective in evaporation of water content of the recovered salt compared to other two heating methods. The absorption band at 3429 cm^{-1} shows a small amount of water in the recovered salts.

3.3.3. Microstructural and elemental analyses

To gain appropriate insight into the morphological and elemental information of the recovered salts by three types of heating sources, FESEM/EDS analyses were used. **Figure 8** depicts the FESEM images and corresponding EDS elemental analyses of the recovered salts. **Figure 8a** shows that the evaporation of water of the leached salt from the ABD through heating by a hotplate has caused the formation of a needle-like nanostructure on surfaces of relatively larger particles (a few to several microns) that seems to be amorphous. Observations at high magnification (**Figure 8a1**), however, reveals that the relatively large particles are aggregation of numerous round shape nanoparticles with a diameter in the range of 33–40 nm. As it can be clearly seen from **Figure 8b**, a pure needle-like morphology has emerged due to the removal of water of the leached salt by microwave heating. **Figure 8b1** shows that the needle-like particles grown with different orientations are in nano scale. The nano-needles show diameter of the tip and base in the range of 39–60 nm and 50–103 nm, respectively. This is despite the fact that the evaporation of water of the leached salt through heating by a drying oven has resulted in the formation of aggregates of round shape nanoparticles only. As can obviously be observed from **Figure 8c**, the agglomerates include nanoparticles with the sizes larger than 20 nm (as shown in **Figure 8c1**). All EDS elemental analyses disclosed Na, F, O, Cl, Al, C, Si, and K as the chemistry of the formed nanostructures.

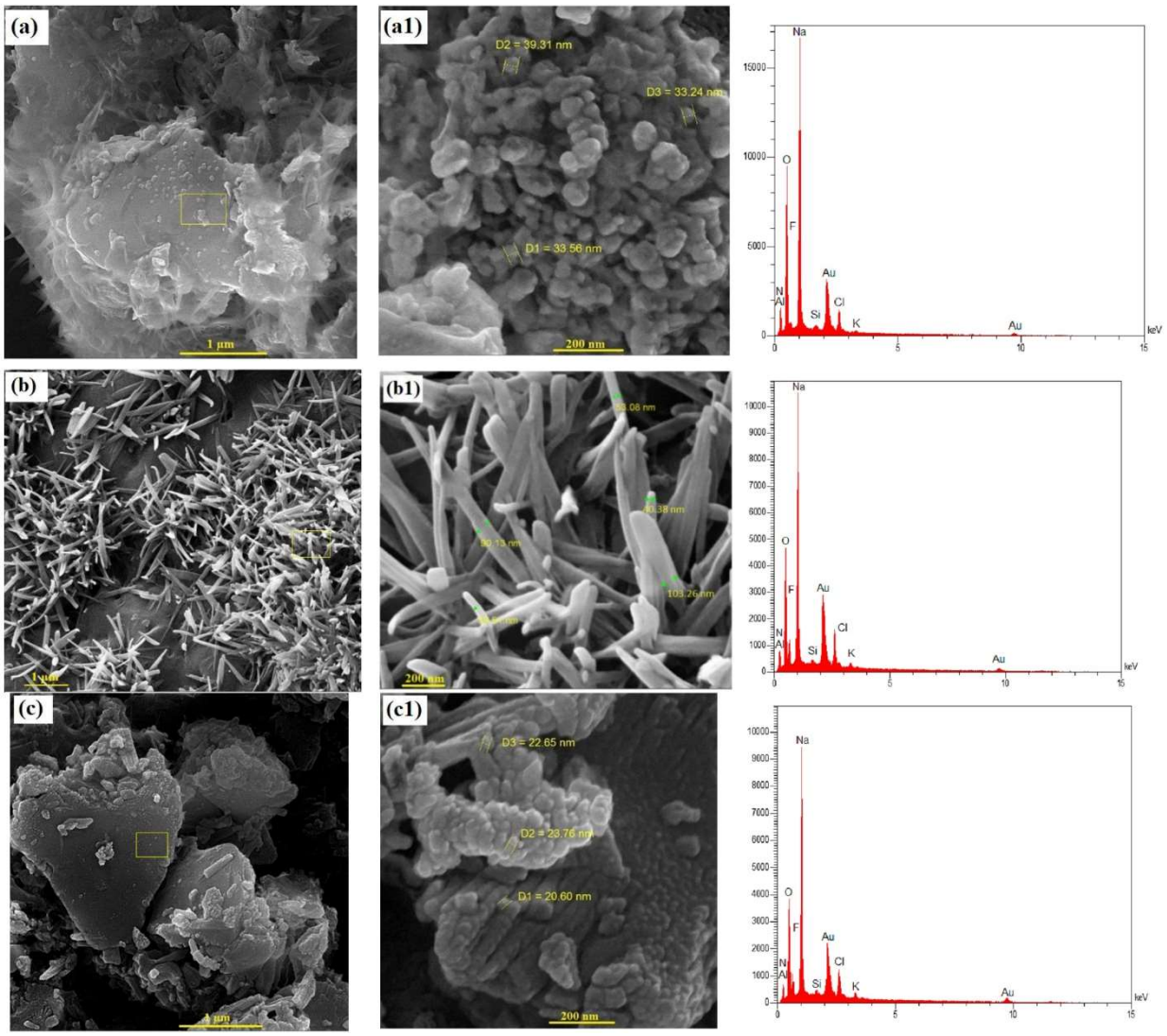

Figure 8. FESEM images and corresponding EDS elemental analyses of the recovered salts. Heat source: **(a, a1)** hotplate; **(b, b1)** microwave irradiation; and **(c, c1)** drying oven.

The mechanism for the formation of different nanostructures can be interpreted as follows:

Water-soluble halides are ionized in water according to the following reaction [16]:

$$NaY_{(solid)} \leftrightarrow Na^{+}_{(aqueous)} + Y^{-}_{(aqueous)} \quad (3)$$

Driving force for the formation of nanostructures of sodium halides or any water-soluble particles is the evaporation of water from a confined space which allows the size and shape control. Considering the type of heating source for evaporation of water of the leached salts, two main parameters that may have a key role in the appearance of different nanostructures are temperature gradient and supersaturation. As shown in **Figure 3**, heating through a hotplate causes the temperature of regions from the solution close to the hot plate to be higher than the temperature of the surface regions of the solution in the vicinity of the air. This results in the formation of a sharp temperature gradient in the solution, which in turn leads to a different evaporation rate and, ultimately, a different crystallization rate. The heat generated by a drying oven with heating elements embedded in top and bottom of the oven chamber creates a

milder temperature gradient compared to the previous heating state. Consequently, the evaporation rate and the rate of crystallization are more uniform. As a result, morphology is expected to be more uniform. Also, the nanoparticles obtained by drying oven and hotplate heating methods tend to severe agglomeration [28] and this is clear in **Figure 8a,c**. The microwave heating as a green heating method, has a mechanism fundamentally different from the common heating methods. This difference is significant from two perspectives: firstly, in common heating methods, i.e., conduction, convection, and radiation, heat is supplied through an external source. While in microwave heating, heat generated from microwave energy is absorbed by the material depending on its position in the microwave field. Secondly, common heating methods produce a sharp temperature gradient in the material, while the microwave heating method does not create any temperature gradient and the temperature of the whole material is almost the same. In addition, microwaves deliver heat uniformly and simultaneously throughout the bulk of a material and also have the potential to penetrate deeply into material bulk [34,35]. As another important reason, experimental results have revealed that the crystal characteristics such as size distribution, crystal morphology and degree of agglomeration are also strongly influenced by the degree of supersaturation at the beginning of crystallization [29,36]. The crystals in a relatively high supersaturated solution focus on extending along the longitudinal direction. With the progress of the process, the supersaturation descends around the tips of the crystals and this causes the tips have a smaller diameter than the bases. As a result, a more orderly and uniform structure is expected.

4. Conclusions

In the present work, NaF-Na_2CO_3-NaCl ternary fluxing agent ternary was recovered from aluminum black dross as a hazardous solid waste. Despite a significant reduction in waste toxicity, the recovery of fluxing agent in the form of a nanostructured salt can provide economic benefits. The recovery process was performed using water as a green solvent followed by the evaporation of water. The heat for the evaporation process was supplied using three sources of heating including a hotplate, microwave irradiation, and a drying oven. Investigating the effects of time and temperature revealed that a recovery efficiency of 96.5% can be achieved under optimum temperature and time of 95 ℃ and 90 min, respectively. The recovered fluxing agent salt was found to contain more than 74 wt.% of NaF by employing the Rietveld fitting analysis. Microstructural study by FESEM disclosed that the ternary fluxing agent has been recovered in the form of highly aggregated round shape nanoparticles, needle-like nanoparticles, and a combination of both.

Author contributions: Conceptualization, MM; methodology, MM; software, MM; validation, MM and AA; formal analysis, MM; investigation, MM and AA; resources, MM and AA; data curation, MM and AA; writing—original draft preparation, MM; writing—review and editing, MM and AA; visualization, MM; supervision, AA; project administration, MM and AA; funding acquisition, MM and AA. All authors have read and agreed to the published version of the manuscript.

Conflict of interest: The authors declare no conflict of interest.

References

1. Xiao Y, Reuter MA, Boin UDO. Aluminium Recycling and Environmental Issues of Salt Slag Treatment. Journal of Environmental Science and Health, Part A. 2005; 40(10): 1861-1875. doi: 10.1080/10934520500183824
2. Tsakiridis PE, Oustadakis P, Agatzini-Leonardou S. Aluminium recovery during black dross hydrothermal treatment. Journal of Environmental Chemical Engineering. 2013; 1(1-2): 23-32. doi: 10.1016/j.jece.2013.03.004
3. Dash B, Das BR, Tripathy BC, et al. Acid dissolution of alumina from waste aluminium dross. Hydrometallurgy. 2008; 92(1-2): 48-53. doi: 10.1016/j.hydromet.2008.01.006
4. Sarker MdSR, Alam MdZ, Qadir MdR, et al. Extraction and characterization of alumina nanopowders from aluminum dross by acid dissolution process. International Journal of Minerals, Metallurgy, and Materials. 2015; 22(4): 429-436. doi: 10.1007/s12613-015-1090-2
5. Unlü N, Drouet MG. Comparison of salt-free aluminum dross treatment processes. Resour Conserv Recycl. 2002; 36. doi: 10.1016/S0921-3449(02)00010-1
6. Yoshimura HN, Abreu AP, Molisani AL, et al. Evaluation of aluminum dross waste as raw material for refractories. Ceramics International. 2008; 34(3): 581-591. doi: 10.1016/j.ceramint.2006.12.007
7. Narayanan R, Sahai Y. Chemical Interactions of Dross with Water and Water Vapor in Aluminum Scrap Remelting. Materials Transactions, JIM. 1997; 38(1): 85-88. doi: 10.2320/matertrans1989.38.85
8. Das BR, Dash B, Tripathy BC, et al. Production of η-alumina from waste aluminium dross. Minerals Engineering. 2007; 20(3): 252-258. doi: 10.1016/j.mineng.2006.09.002
9. Shinzato MC, Hypolito R. Solid waste from aluminum recycling process: characterization and reuse of its economically valuable constituents. Waste Management. 2005; 25(1): 37-46. doi: 10.1016/j.wasman.2004.08.005
10. Harrison PTC. Fluoride in water: A UK perspective. Journal of Fluorine Chemistry. 2005; 126(11-12): 1448-1456. doi: 10.1016/j.jfluchem.2005.09.009
11. World Health Organization. Sodium in drinking-water, background document for development of WHO guidelines for drinking-water quality, 2nd ed. World Health Organization; 1996.
12. Bruckard WJ, Woodcock JT. Recovery of valuable materials from aluminium salt cakes. International Journal of Mineral Processing. 2009; 93(1): 1-5. doi: 10.1016/j.minpro.2009.05.002
13. Afzal S, Rahimi A, Ehsani MR, et al. Experimental study of hydrogen fluoride adsorption on sodium fluoride. Journal of Industrial and Engineering Chemistry. 2010; 16(1): 147-151. doi: 10.1016/j.jiec.2010.01.004
14. Fryxell GE, Cao G. Environmental Applications of Nanomaterials. Imperial College Press; 2011. doi: 10.1142/p814
15. Lailach G, Bulan A, Buss G. Process for the preparation of sodium fluoride. US6251358B1, 1998.
16. Abdelkader E, Buckner SW. Synthesis of NaX (X = F, Cl, Br, I) Nanoparticles. Soft Nanoscience Letters. 2013; 3(1): 22-27. doi: 10.4236/snl.2013.31005
17. Kupka N, Rudolph M. Role of sodium carbonate in scheelite flotation—A multi-faceted reagent. Minerals Engineering. 2018; 129: 120-128. doi: 10.1016/j.mineng.2018.09.005
18. Kientzler P, Löbbers K, Michard L. Improved modifying flux for molten aluminium. EP2231887A1, 2013.
19. Dang H, Chang Z, Wu X, et al. Na_2SO_4–NaCl binary eutectic salt roasting to enhance extraction of lithium from pyrometallurgical slag of spent lithium-ion batteries. Chinese Journal of Chemical Engineering. 2022; 41: 294-300. doi: 10.1016/j.cjche.2021.09.008
20. Huang J, Wang Y, Zhou G, et al. Investigation on the Effect of Roasting and Leaching Parameters on Recovery of Gallium from Solid Waste Coal Fly Ash. Metals. 2019; 9(12): 1251. doi: 10.3390/met9121251
21. Wu H, Yan H, Liang Y, et al. Rare earth recovery from fluoride molten-salt electrolytic slag by sodium carbonate roasting-hydrochloric acid leaching. Journal of Rare Earths. 2023; 41(8): 1242-1249. doi: 10.1016/j.jre.2022.07.001
22. Anastas PT, Warner JC. Green Chemistry: Theory and Practice. Oxford University Press; 1998.
23. Mahinroosta M, Allahverdi A. A promising green process for synthesis of high purity activated-alumina nanopowder from secondary aluminum dross. Journal of Cleaner Production. 2018; 179: 93-102. doi: 10.1016/j.jclepro.2018.01.079
24. Mahinroosta M, Allahverdi A. Enhanced alumina recovery from secondary aluminum dross for high purity nanostructured γ-alumina powder production: Kinetic study. Journal of Environmental Management. 2018; 212: 278-291. doi: 10.1016/j.jenvman.2018.02.009

25. Bowen P, Highfield JG, Mocellin A, et al. Degradation of Aluminum Nitride Powder in an Aqueous Environmet. Journal of the American Ceramic Society. 1990; 73(3): 724-728. doi: 10.1111/j.1151-2916.1990.tb06579.x
26. Fukumoto S, Hookabe T, Tsubakino H. Hydrolysis behavior of aluminum nitride in various solutions. J Mater Sci. 2000; 35. doi: 10.1023/A:1004718329003
27. Reynolds JG, Belsher JD. A Review of Sodium Fluoride Solubility in Water. Journal of Chemical & Engineering Data. 2017; 62(6): 1743-1748. doi: 10.1021/acs.jced.7b00089
28. Wang B, Zhang W, Zhang W, et al. Progress in Drying Technology for Nanomaterials. Drying Technology. 2005; 23(1-2): 7-32. doi: 10.1081/drt-200047900
29. Sarig S, Eidelman N, Glasner A, et al. The effect of supersaturation on the crystal characteristics of potassium chloride. Journal of Chemical Technology and Biotechnology. 1978; 28(10): 663-667. doi: 10.1002/jctb.5700281004
30. Balasubramanian C, Bellucci S, Cinque G, et al. Characterization of aluminium nitride nanostructures by XANES and FTIR spectroscopies with synchrotron radiation. Journal of Physics: Condensed Matter. 2006; 18(33): S2095-S2104. doi: 10.1088/0953-8984/18/33/s25
31. Roy Chowdhuri A, Takoudis CG, Klie RF, et al. Metalorganic chemical vapor deposition of aluminum oxide on Si: Evidence of interface SiO_2 formation. Applied Physics Letters. 2002; 80(22): 4241-4243. doi: 10.1063/1.1483903
32. Bryukvina LI, Khulugurov VM, Parfianovich IA. Infrared vibrational spectra of radiatively induced absorption of NaF: OH crystals. Opt Spectrosc. 1987; 63(1).
33. Cheng J, Guo R, Wang QM. Zinc oxide single-crystal microtubes. Applied Physics Letters. 2004; 85(22): 5140-5142. doi: 10.1063/1.1825067
34. Cheng J, Agrawal D, Zhang Y, et al. Fabricating transparent ceramics by microwave sintering. Am Ceram Soc Bull. 2000; 79(9).
35. Liu XY, Bennema P. Theoretical consideration of the growth morphology of crystals. Physical Review B. 1996; 53(5): 2314-2325. doi: 10.1103/physrevb.53.2314
36. Ma M, Ye W, Wang XX. Effect of supersaturation on the morphology of hydroxyapatite crystals deposited by electrochemical deposition on titanium. Materials Letters. 2008; 62(23): 3875-3877. doi: 10.1016/j.matlet.2008.05.009